Dynamic Aeroelastic Simulation of the AGARD 445.6 Wing using Edge

POYAN PAHLAVANLOO

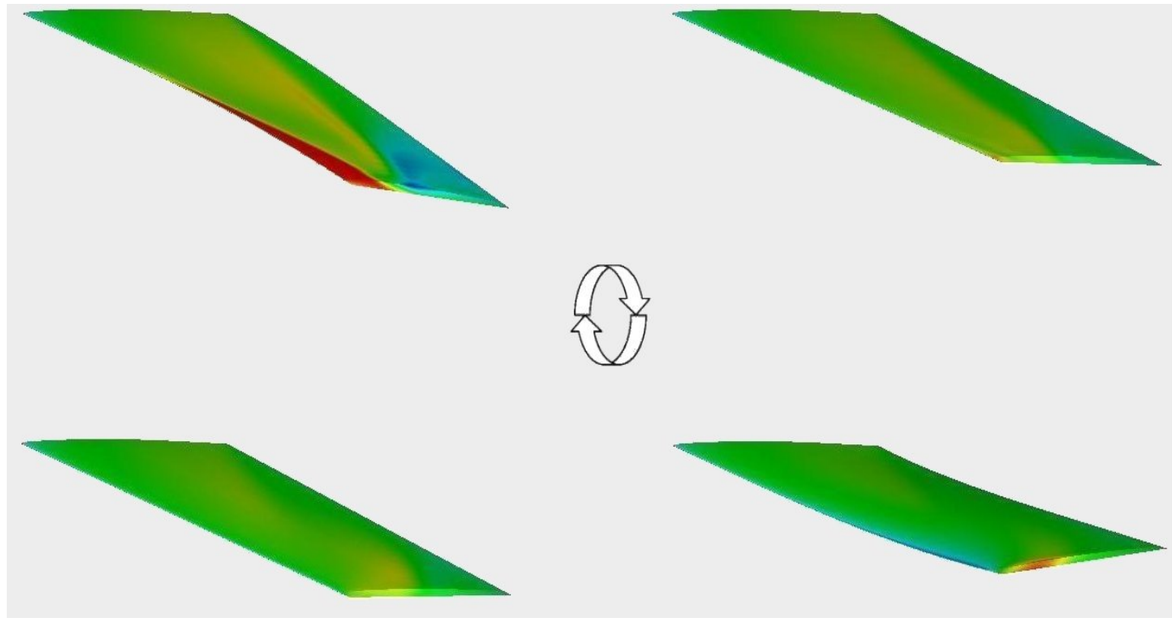

FOI
Defence Research Agency
Defence and Security, Systems and Technology
SE-164 90 Stockholm

Phone: +46 8 555 030 00
Fax: +46 8 555 031 00

www.foi.se

FOI-R--2259--SE
ISSN 1650-1942

Technical report
April 2007

Defence and Security, Systems and Technology

Poyan Pahlavanloo

Dynamic Aeroelastic Simulation of the AGARD 445.6 Wing using Edge

FOI-R--2259--SE Technical report
ISSN-1650-1942 April 2007

Defence and Security, Systems and Technology

Issuing organisation FOI – Swedish Defence Research Agency Defence and Security, Systems and Technology SE-164 90 STOCKHOLM	**Report number, ISRN** FOI-R--2259--SE	**Report type** Technical report
	Research area code Mobility and Space Technology, incl Materials	
	Month year April 2007	**Project no.** B66004
	Sub area code 79. Interdisciplinary Projects...	
	Sub area code 2	

Author/s (editor/s) Poyan Pahlavanloo	**Project manager** Olivier Amoignon
	Approved by Helena Bergman
	Sponsoring agency Swedish Defence Materiel Administration
	Scientifically and technically responsible Jonathan Smith

Report title
Dynamic Aeroelastic Simulation of the AGARD 445.6 Wing using Edge

Abstract
Time-accurate aeroelastic simulations have been carried using the modal coupled aeroelastic implementation in Edge for a standard experimental test case: the AGARD 445.6 aeroelastic wind-tunnel model. The objective has been to provide additional validation of the aeroelastic functionality in Edge and to investigate the different flutter mechanisms in the subsonic and transonic regions. The simulation results, both in flutter frequency and flutter speed are in good agreement with experiments and other simulations and produce the expected “transonic dip” at Mach 0.96. Final analysis show that the flutter motion in the subsonic region is characterized as classical flutter with a combination of the wing-bending and wing-torsion modes, while the transonic flutter is characterized as a single bending mode instability.

Keywords
Aeroelasticity, Edge, CFD, AGARD 445.6, aerodynamic damping, transonic flutter, FSI, LCO, flutter boundary, flutter mechanism

Further bibliographic information	**Language** English
ISSN ISSN-1650-1942	**Pages** 26 p.
	Price acc. to pricelist

Utgivare FOI – Totalförsvarets forskningsinstitut Försvars- och säkerhetssystem 164 90 STOCKHOLM	**Rapportnummer, ISRN** FOI-R--2259--SE	**Klassificering** Teknisk rapport
	Forskningsområde Ledning och MSI	
	Månad år April 2007	**Projektnummer** B66004
	Delområde 79. Breda projekt...	
	Delområde 2	
Författare/redaktör Poyan Pahlavanloo	**Projektledare** Olivier Amoignon	
	Godkänd av Helena Bergman	
	Uppdragsgivare/kundbeteckning FMV	
	Tekniskt och/eller vetenskapligt ansvarig Jonathan Smith	

Rapportens titel
Dynamisk Aeroelastiska Simuleringar på AGRAD 445.6 vingen med Edge

Sammanfattning
Tidsnoggranna, modalkopplade, aeroelastiska simuleringar har genomförts i Edge för ett standard experiment testfall: AGARD 445.6 aeroelastisk vindtunnel model. Anledningen med denna studie är att tillföra ytterligare validering av aeroelastiska funktionaliteten i Edge, samt att undersöka fladdermekanismen i det subsoniska och transoniska området. Simuleringsresultaten i både fladderfrekvens och fladdderhastighet är i god enighet med experimentella värden och andra liknande simuleringar, och producerar det förväntade "transonic dip" (sänkning i fladderhastighet) vid Mach 0.96. Analyser visar att fladderrörelsen i subsoniska området är karakteriserad som klassisk fladder med kombination av vingens böj- och torsionsmoder, medan fladdret i transoniska området är karakteriserad som en enkel instabilitet i första böjmoden.

Nyckelord
Aeroelasticitet, Edge, CFD, AGARD 445.6, aerodynamisk dämpning, transonisk fladder, FSI, LCO, fladdergräns, fladdermekanism

Övriga bibliografiska uppgifter	**Språk** Engelska
ISSN ISSN-1650-1942	**Antal sidor:** 26 s.
Distribution enligt missiv	**Pris: Enligt prislista**

Contents

Acknowledgments

All simulations were performed at the Swedish Defence Research Agency, FOI, in Kista. I would like to acknowledge my supervisor at FOI, Jonathan Smith, for his patient guidance and open door policy. I would also like to thank Peter Eliasson, the principal developer of Edge, and Dan Borglund, my examiner at KTH, for helpful advice.

1 Introduction

An aeroelastic implementation was introduced in Edge version 3.3.1, released in May 2005. As a standard procedure, the functionality of the aeroelastic code needs to be validated with other simulations and more importantly, with aeroelastic experiments. In the initial work by Smith [9], the Edge code was evaluated with experiments with prescribed, rigid-pitch motion (the LANN-wing) and a code-to-code comparision of coupled aeroelastic simulations (the MDO-wing). In the same paper, recommendations were given for additional validation study of the code's modal-coupled implementation for the AGARD 445.6 aeroelastic wind-tunnel model.

This report is an addendum to the initial validation study and presents an analysis of the flutter boundary for the AGARD wing in subsonic and supersonic regions, including investigations of different flutter mechanisms. This paper is a condensed version of Pahlavanloo's M.Sc. thesis [8]. The computational procedure is decribed in detail in [9, 12].

2 The AGARD 445.6 Test Case Description

2.1 AGARD 445.6 Experiments

In the early 1960s, experimental flutter tests were performed in the Langley transonic dynamics tunnel in Hampton, Virginia, known as the AGARD 445.6 dynamic aeroelastic test cases. A series of subsonic and transonic flutter data were obtained on different wing models in both air and Freon-12. We consider the experiments performed in air on the wind-tunnel model denoted 'weakened 3' [10]. This specific model had a profile as the symmetric NACA 65A004 in the streamwise direction, with a 4% profile thickness. The wing had a sweep angle of 45 degrees at the quarter chord line, a semi-span of 0.762 m, and a taper ratio of 0.66. The wing planform and profile are shown in Figure 2.1.

The experiments were performed with the uncambered model rigidly mounted on the tunnel wall, at a zero angle of incidence, thus eliminating any static aeroelastic deformation. Table 2.1 presents the experimental data at flutter for the above selected configuration, where ρ_f, V_f, q_f and ω_f denote the density, speed, dynamic pressure and frequency at the flutter threshold.

Transonic aeroelastic experiments are extremely expensive and the AGARD test cases were, and still are one of the few experimental flutter test available in the public domain.

2.2 AGARD 445.6 Modal Data

Modal data for the wind-tunnel model, in the form of the frequencies of its first six natural modes and their corresponding mode shapes are also provided in [10]. Ground Vibration Tests (GVT) were carried out for detecting the models natural modes [5]. Information about the material properties, together with the natural modes were used in finite-element analysis to calculate the corresponding mode shapes [11]. These are defined in 121 points on the surface, and are normalized so that the generalized mass equals one in units lbf-in-s^2. This corresponds to 0.112979 kgm^2 in SI units. Figure 2.2 illustrates the first six modeshapes and their natural frequencies which are used in the computations presented here. For the Edge calculations, these mode shapes are transformed from the structural grid to displacements on the CFD grid, see reference [9] for details.

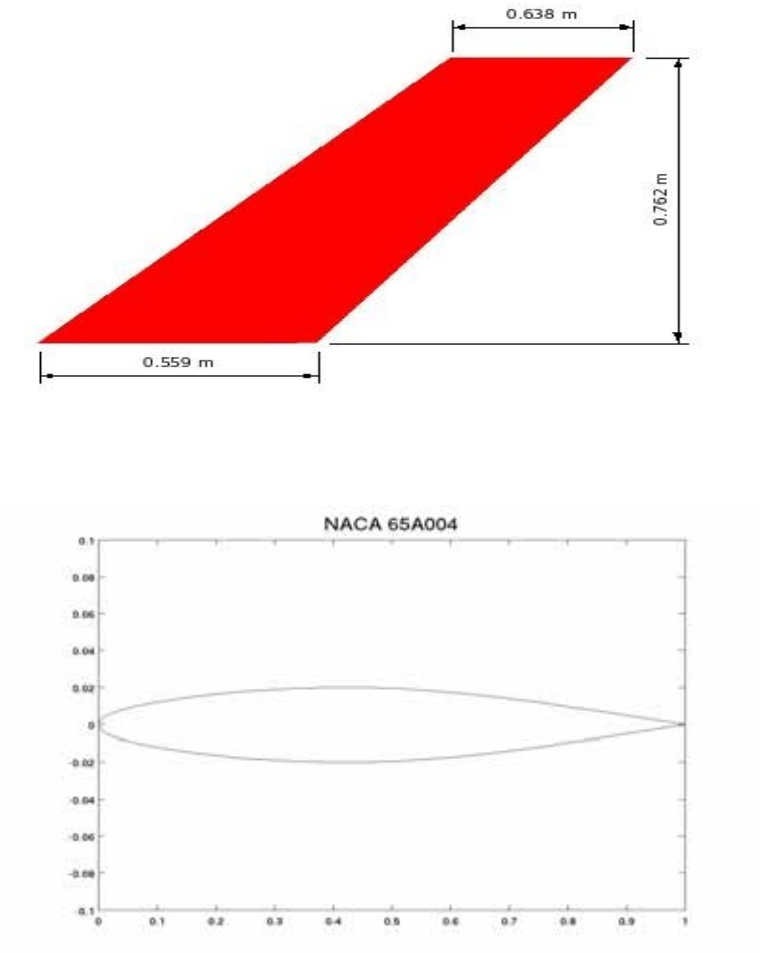

Figure 2.1: AGARD 445.6 planform and profile.

Mach	ρ_f $[kg/m^3]$	V_f m/s	q_f [Pa]	ω_f $[rad/s]$
0.499	0.42770	172.5	6375	128.1
0.678	0.20818	231.4	5542	113.0
0.901	0.09945	296.7	4277	101.1
0.954	0.06338	307.4	2903	91.1
0.957	0.06338	311.0	2955	87.9
0.960	0.06338	309.0	2936	87.3
1.072	0.05514	344.7	3166	86.7
1.141	0.07833	364.3	5044	109.9

Table 2.1: Experimental flutter data for 'weakened 3' [10].

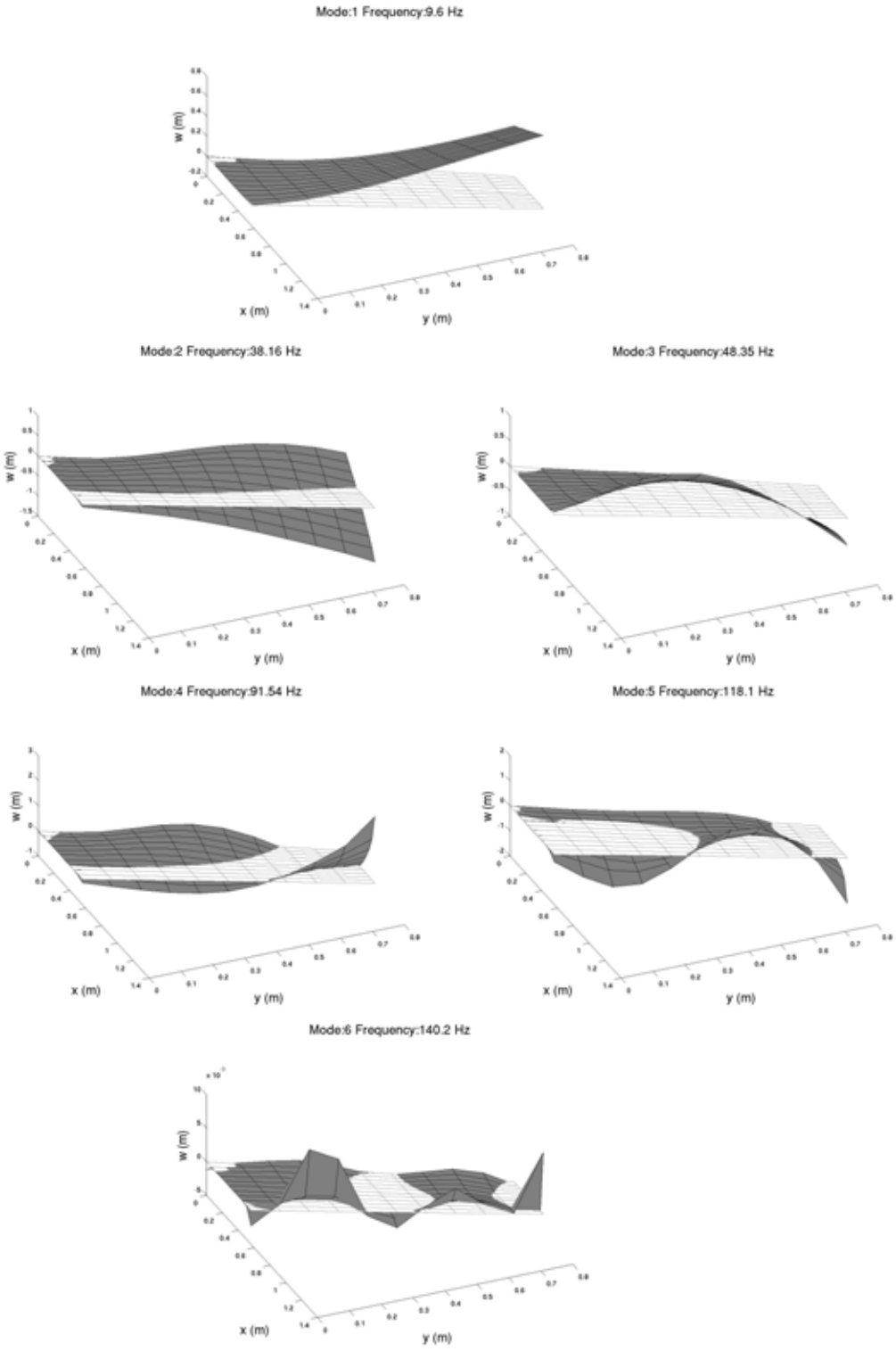

Figure 2.2: First six mass-normalized vibration modes.

3 Flutter Boundary Location

3.1 Damping Estimation

Each aeroelastic calculation in Edge is similar to a single flight test with specific aerodynamic conditions, providing a time-domain impulse response for the coupled aeroelastic system. The impulse response can be analysed to obtain estimate of the response frequency and the aerodynamic damping. However, to locate the flutter boundary, an analysis of several of these calculations is required.

From a single response it is possible to estimate a damping ratio, ζ_e, yielding positive damping for convergent solutions (stable), and negative damping for divergent solutions (unstable). The damping of the response is the combined structural and aerodynamic damping. However, for the dynamic calculations presented here, the structural damping has been set to zero, so ζ_e is purely the aerodynamic damping.

The impulse response can be the generalized coordinates of each mode, or their combined effect in the real-space displacement of a reference point on the wing. For a free-decaying, damped oscillation, such as that shown in Figure 3.1, the aerodynamic damping, ζ_e, can be derived from a quantity known as the *logarithmic decrement* [7]

$$\delta_n = \frac{1}{n} ln \left(\frac{X_i}{X_{i+n}} \right) = \frac{2\pi\zeta_e}{\sqrt{1-\zeta_e^2}}, \tag{3.1}$$

where referring to this figure, X_i is the peak amplitude at a certain instant of time and X_{i+n} is the peak amplitude taken after n complete cycles of vibration. For a pure, exponential, convergent or divergent oscillation, the logarithmic decrement, δ_n, in equation (3.1) is independent of n. This is, however, not exactly true for a time-domain response from Edge, since the response is not a pure exponential oscillation.

A Matlab function has been developed in order to map the region of the impulse response which is most similar to an exponential oscillation, and thereafter estimate the damping from equation (3.1). This function is now available in the Edge Matlab package.

Damping estimations are collected for a large set of test points at constant Mach numbers. The flutter boundary is then located using linear interpolation to find the dynamic pressure for which $\zeta_e = 0$. Since this method is dependent of the test points closest to $\zeta_e = 0$, accuracy in the flutter boundary is improved by refining the search with more test points as described in section 3.2.

3.2 Simulation Test Points

To simulate the wind-tunnel tests, flutter calculations are carried out based on variation in dynamic pressure at constant Mach numbers. This is done by using the experimental velocity and varying the density. To locate the flutter

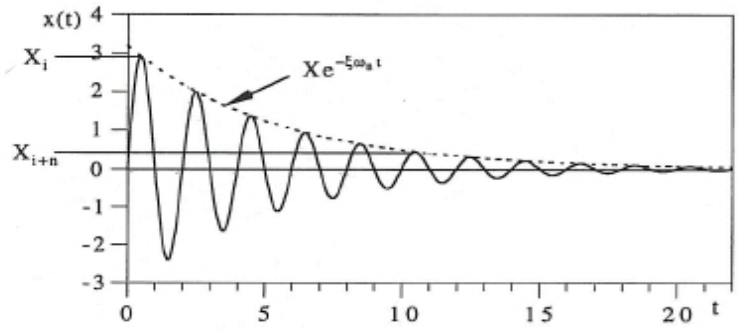

Figure 3.1: Free damped decaying system, $i = 1$ and $n = 5$.

boundary, several dynamic pressures are chosen near the experimental values, both in the stable and unstable region.

Figure 3.2 shows the experimental flutter curve together with the distribution of numerical test points. Six of the selected free-stream Mach numbers are

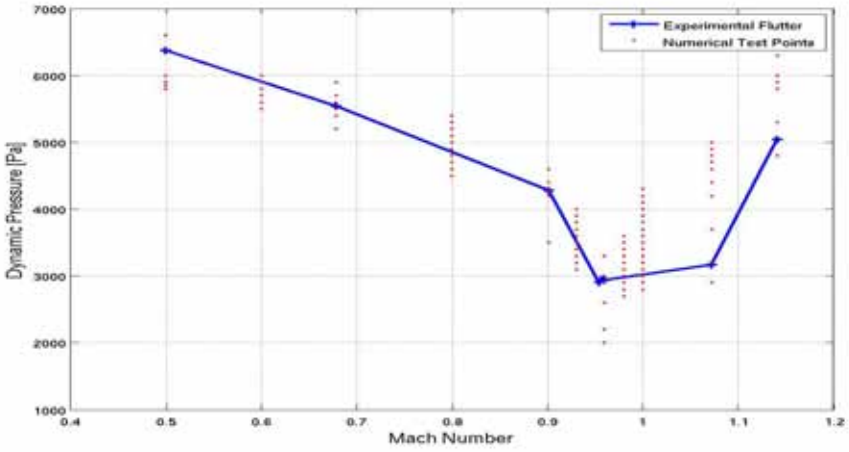

Figure 3.2: Experimental flutter and distribution of numerical test points.

identical to the experimental values in Table 2.1. However, to gain an increased resolution, five additional constant-Mach series are added, two in the subsonic region, $M = 0.6, 0.8$, and three in the transonic region, $M = 0.93, 0.98, 1.0$. At each Mach number, calculations are performed for all chosen dynamic pressures, making a total of 182 static and dynamic simulations.

4 Simulation Results

The results presented here are based on unsteady Euler computations using a CFD mesh with 1.4e5 nodes. This mesh is converted from the structured EURANUS[1] mesh that was used in an earlier study within the EU-project UNSI [4].

4.1 Static Coupled Simulations

The first step in the simulations is to obtain a static aeroelastic solution, i.e. solutions where the fluid loads and the elastic restoring forces are in static equilibrium. This is done by setting the structural damping to unity, thus eliminating any oscillatory response. With a physical timestep of $\Delta t = 5$ ms convergence is reached in less than 0.2 s of model time, resulting in computational costs comparable to those of a conventional, rigid, steady-state solution.

Figure 4.1 shows the generalized modal coordinates for the case $M_\infty = 0.499$ and $q_{dyn} = 5800$ Pa, where it is clearly seen that the static response is mainly dominated by the first and second structural modes.

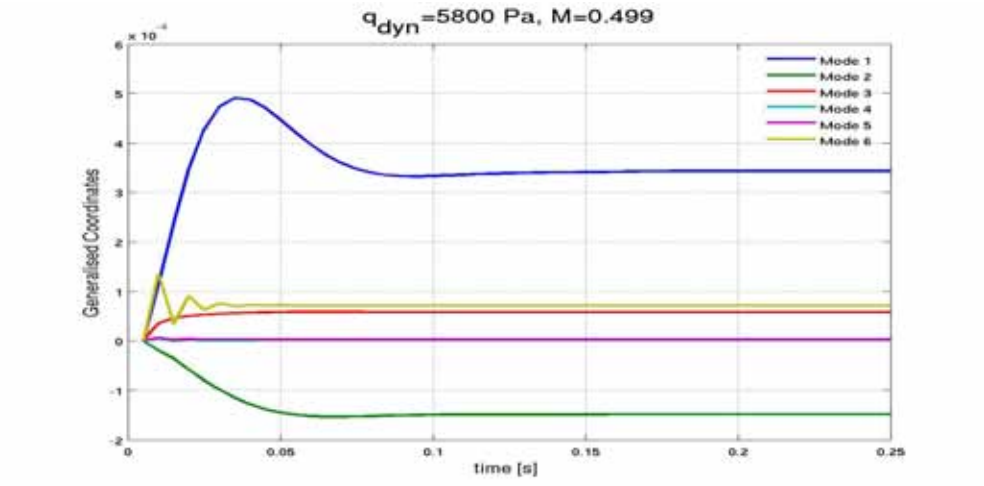

Figure 4.1: Static Response of the generalized coordinates for the case $M_\infty = 0.499$ and $q_{dyn} = 5800$ Pa.

Figure 4.2 shows the real-space, vertical displacement of the wing-tip trailing edge for the same case as in Figure 4.1. The displacement is of a magnitude $\sim 10^{-4}$ m, which is negligible static deformation on a 0.76 m wing.

Similar results were obtained for all the static simulations. This is consistent with the observation in section 2.1, that due to the symmetric wing profile, the static deflection at zero incidence should be zero. The small deflection

[1] FFA-developed, structured multiblock flow-solver with aeroelastic functionality.

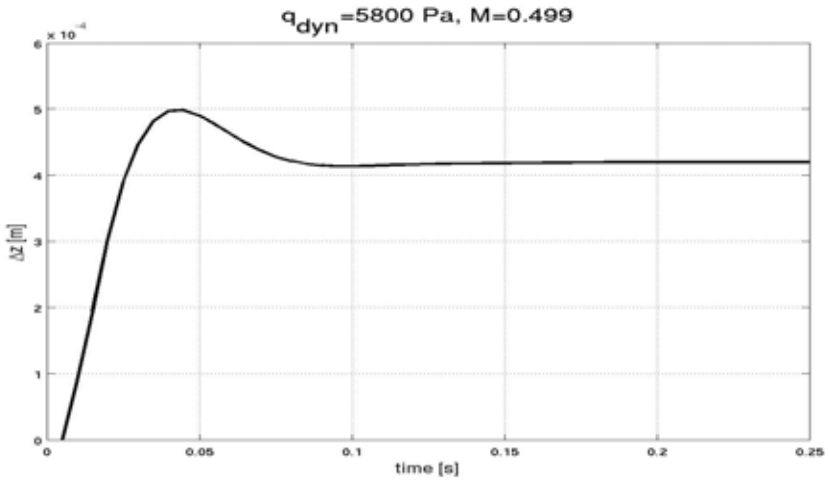

Figure 4.2: Static vertical displacement for wing-tip trailing edge for the case $M_\infty = 0.499$ and $q_{dyn} = 5800$ Pa.

observed is probably due to a slight, vertical asymmetry, arising from the coarse resolution of the CFD grid.

4.2 Dynamic Coupled Simulations

Dynamic coupled simulations are performed starting from the static-equilibrium solutions and a structural excitation is introduced by setting a non-zero initial velocity for mode 1. The modal excitation velocity is set to $\dot{q} = 2\pi f_1 q_1$, where q_1 is the modal coordinate corresponding to a vertical displacement of 5 cm at the wing-tip trailing edge, for the undamped "air off" case. Further, the structural damping is set to zero in order to isolate the effects of aerodynamic forces. For all dynamic calculations the timestep is set to $\Delta t = 2$ ms, resolving the highest structural mode to just over 3 points per cycle. The inner loop convergence process is set to a constant 30 iterations throughout.

Typical results from the dynamic simulations are shown in Figures 4.3 to 4.5. Figure 4.3 shows the dynamic response of the generalized coordinates for the case $M_\infty = 0.499$ and $q_{dyn} = 5800$ Pa. This figure shows a stable system, with a response dominated by the first and second structural modes.

Figure 4.4 shows the vertical displacement for the wing-tip trailing edge reference point for the same case as above, together with a frequency response spectrum which is the modulus of its Fourier transform. In the time-history, the initial response peak is approximately 3.5 cm at $t = 0.018$ s, and is followed by the maximum response of -3.9 cm at $t = 0.044$ s. This is much larger than the static response, shown in Figure 4.2, but significantly less than the "air off" amplitude, $\pm$ 5 cm. The aerodynamic damping estimator, described in section 3.1, yields $\zeta_e = 0.017$ for this system. After 0.5 s, the oscillation has decayed to 40 % of the initial maximum. The response spectrum has a single peak at approximately 22.3 Hz, indicating that the wing is behaving as a single DOF system. The response peak is roughly mid-way between the first two structural modes at 9.6 Hz and 38.1 Hz.

Figure 4.5 shows the vertical dynamic response at the wing-tip reference point for the unstable case $M_\infty = 1.0$ and $q_{dyn} = 4300$ Pa. The initial response maximum is 3.9 cm, only slightly larger than for the stable case, shown in Figure 4.4, but after just 0.5 s, the amplitude has increased to approximately 11 cm.

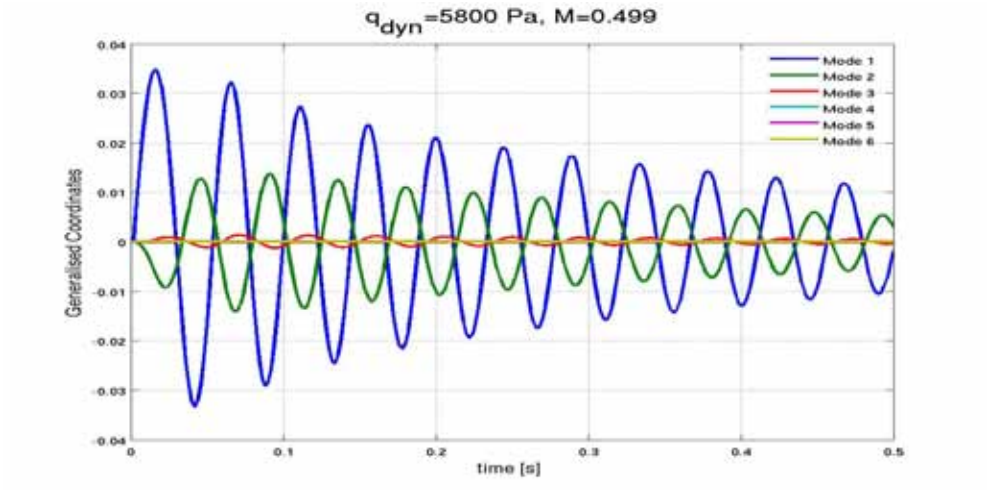

Figure 4.3: Dynamic response of the generalized coordinates for the subsonic stable case $M_\infty = 0.499$ and $q_{dyn} = 5800$ Pa.

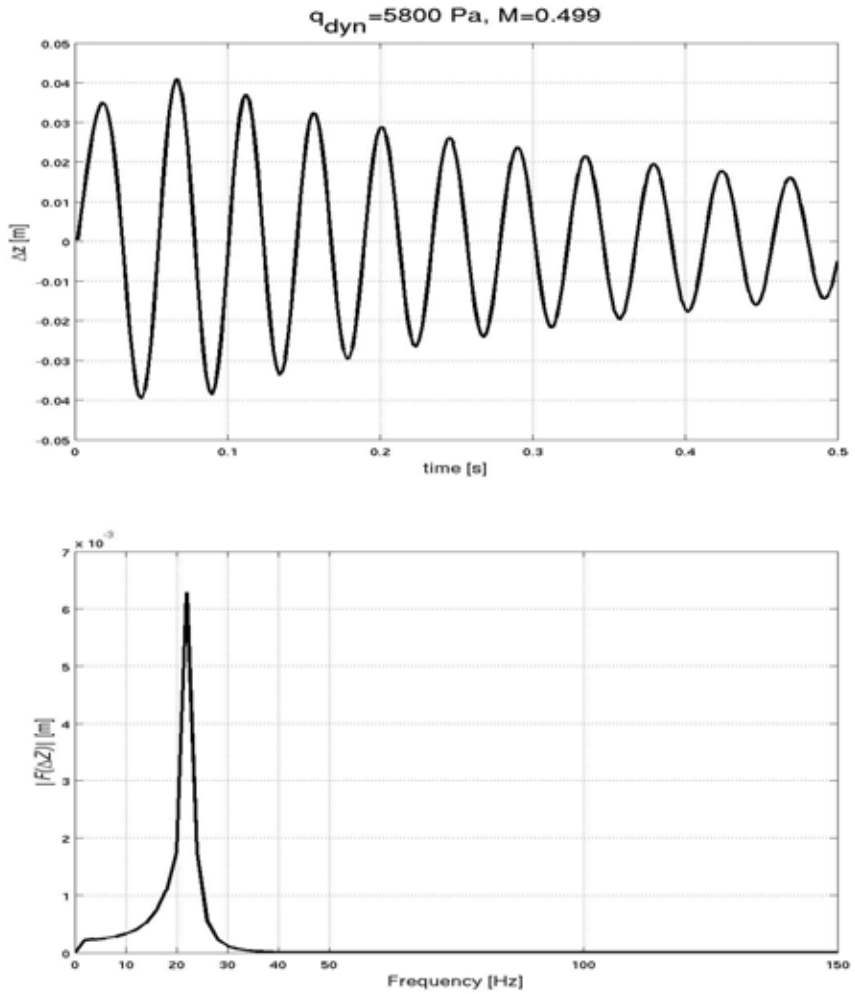

Figure 4.4: Dynamic vertical displacement for wing-tip trailing edge for the subsonic stable case $M_\infty = 0.499$ and $q_{dyn} = 5800$ Pa.

The aerodynamic damping estimate is $\zeta_e = -0.0205$. The frequency spectrum shows a single peak at approximately 16.7 Hz, indicating that the motion is similar to a single DOF system.

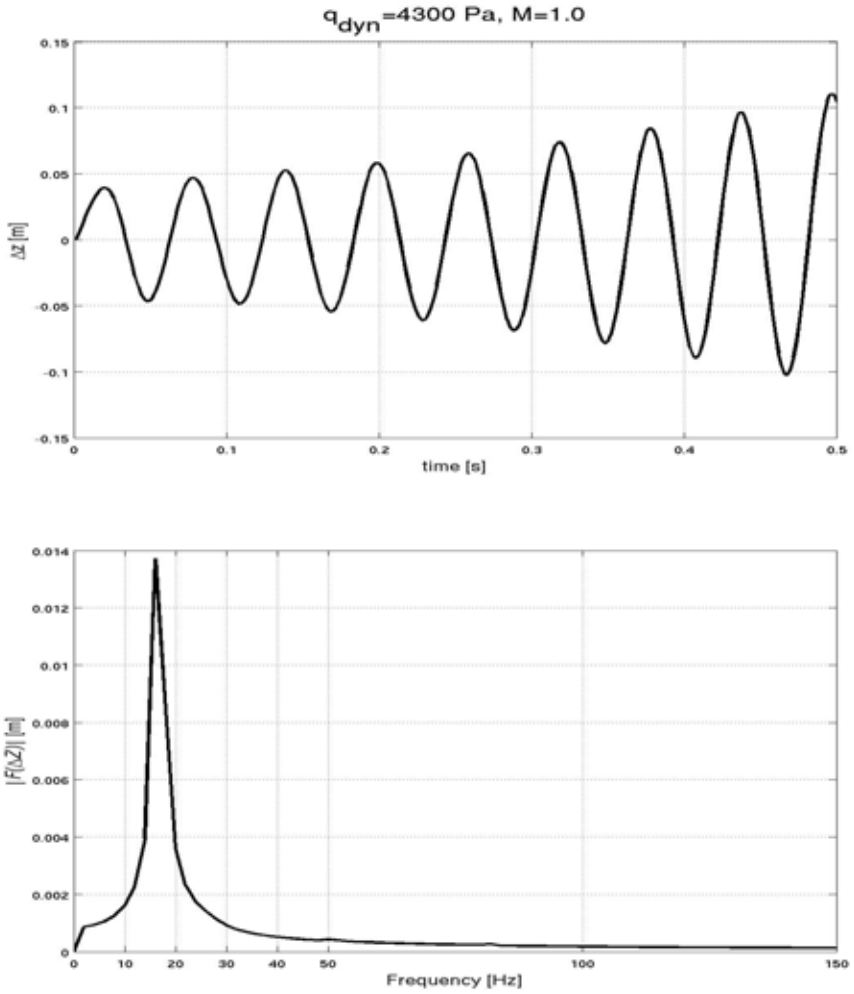

Figure 4.5: Dynamic vertical displacement for wing-tip trailing edge for the transonic unstable case $M_\infty = 1.0$ and $q_{dyn} = 4300$ Pa.

Of the 91 dynamic simulations, 38 showed unstable flutter-like behaviour similar to Figure 4.5. However, none of these solutions showed any evidence of the limiting amplitude characteristics of an LCO. In 12 cases, the amplitude became so large, about 15 cm at the wing-tip trailing edge, that the mesh contained negative cells and the solutions terminated. Our failure to produce an LCO may be due to the sensitivity of the grid. However, the lack of LCO is consistent with other investigations which indicate that no such phenomena arise with the AGARD 445.6 wing [1].

4.3 Aerodynamic Damping Estimation and Flutter Boundary

Having collected response data for all the aeroelastic simulations, it is now appropriate to make estimations of the aerodynamic damping and through this to locate the flutter boundary. This is done using the damping estimator described in section 3.1. The damping of the response of the wing-tip reference

point is obtained as a function of dynamic pressure at each Mach number, and flutter boundary is interpolated at zero aerodynamic damping. This process is illustrated in Figure 4.6.

Figure 4.6 shows the estimated aerodynamic damping, ζ_e, as a function of the dynamic pressure for $M_\infty = 1.0$, together with two insets, each showing typical impulse response for the wing-tip trailing edge reference point, when $\zeta_e > 0$ ($q_{dyn} = 3000$ Pa) and $\zeta_e < 0$ ($q_{dyn} = 4300$ Pa). The aerodynamic damping shows a continuous variation with the dynamic pressure. The interpolation line between the test points closest to $\zeta_e = 0$ is highlighted in blue. The flutter boundary for this Mach number case is interpolated to a value of $q_{dyn} = 3840$ Pa.

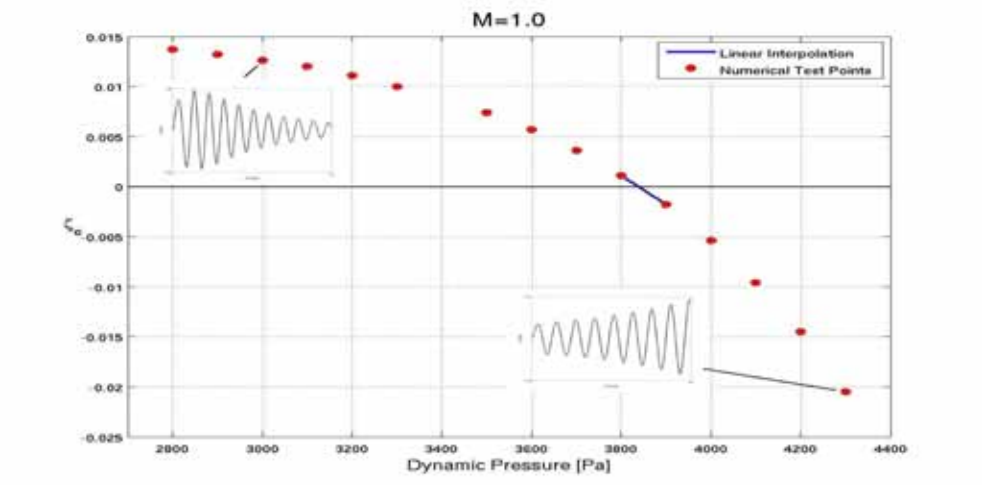

Figure 4.6: Aerodynamic damping as a function of the dynamic pressure for $M_\infty = 1.0$. Insets show impulse response for wing-tip trailing edge, when $q_{dyn} = 3000$ Pa and $q_{dyn} = 4300$ Pa.

Using the same procedure over the full range of Mach numbers, the flutter boundary is estimated and compared to the experimental measurements.

Figure 4.7 shows the experimental flutter boundary together with the computed flutter results from Edge. The diagrams show the dynamic pressure and response frequency at flutter as functions of the free stream Mach number. In both diagrams the broad features in the computed flutter boundary agree closely with the experiments. The transonic dip in particular is captured with excellent precision, in Mach, frequency and dynamic pressure. The dynamic pressure at flutter is in closest agreement with the experiments up to the transonic dip at Mach 0.96, but exceeds the experimental values at higher Mach numbers. This results in a sharper dip compared with the experiments. A similar pattern is evident in the flutter frequency. However, the computed flutter frequencies up to Mach 0.9 are about 10 % higher compared with the experiments. The discrepancy in both flutter dynamic pressure and frequency is largest for the experimental point at Mach 1.072.

Figure 4.8 shows comparative plots of the Edge simulation, together with the experimental data and three other published computation results [4, 6]. The results are shown in terms of the Flutter Speed Index (FSI). The FSI is defined as:

$$FSI = \frac{V_f}{b_s \omega_\alpha \sqrt{\mu}}, \tag{4.1}$$

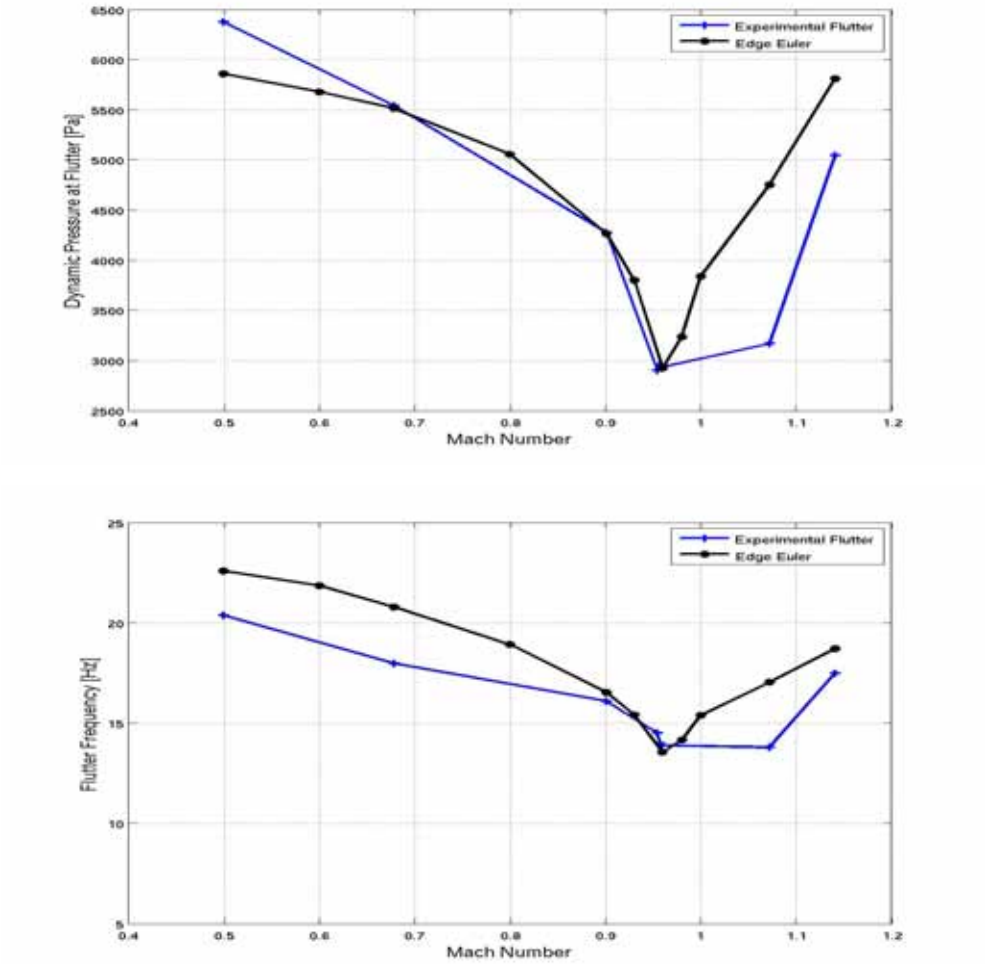

Figure 4.7: Edge flutter results compared with the AGARD experimental data.

where V_f is the flutter speed, b_s is the half root chord, ω_α is the angular frequency of the first torsional mode (mode 2 in Figure 2.2) and μ is the mass ratio, i.e. the ratio between the structural mass and the mass of the equivalent volume of fluid at reference density [10]. The flutter frequency ratio is defined as ω/ω_α.

The results by Saab are based on Euler calculations using the Euranus code with a time-linearisation technique. The flutter results by Batina and Lee-Rauch are based on Euler calculations with a similar time-linearisation technique. Batina and Lee-Rauch located the flutter boundary through damping and frequency estimations in a Modal Identification procedure. DASA-M used a modal coupled, Euler CFD code. The flutter boundary was located through variation in stagnation pressure until the time-dependent solutions showed a neutrally stable character.

The simulation results from Edge, in terms of the speed index and flutter frequency ratio, are in some regions similar to the Euler results from Batina and Lee-Rauch, Saab and DASA-M. These results show the same discrepancy in flutter frequency ratio up to Mach 0.9 as the Edge simulation results. All three methods succeed in capturing the transonic dip, though Edge does this with better precision in both speed index and flutter frequency ratio. The

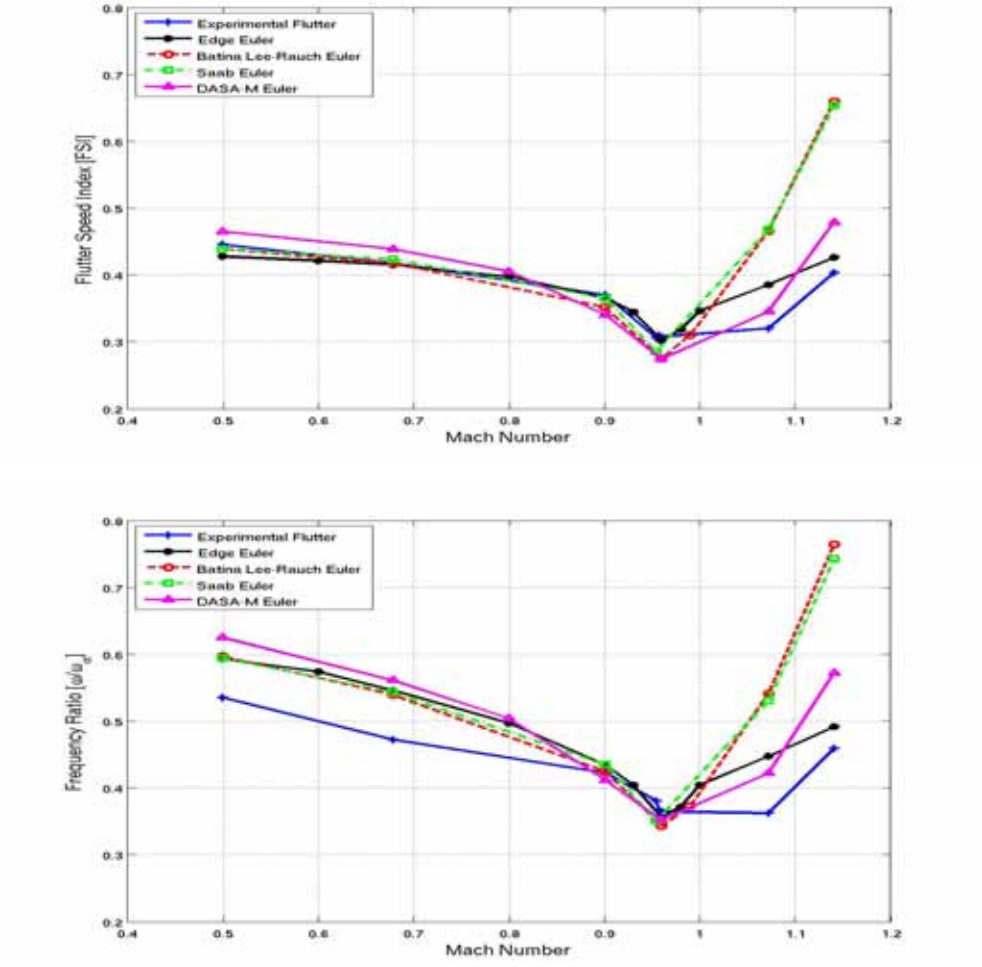

Figure 4.8: Edge flutter results in terms of Flutter Speed Index and flutter frequency ratio in comparison with the AGARD experimental data and inviscid results from literature.

discrepancy in the high transonic region in the speed index and flutter frequency ratio is much smaller in the Edge results, except for the experimental point at Mach 1.072, where DASA-M is closest to the experiment flutter boundary. The discrepancies against the experimental flutter boundary in terms of the speed index in the high transonic region and the flutter frequency ratio in the low subsonic and high transonic regions are similar to other viscid and inviscid simulations [4, 1, 3].

5 Flutter Mechanisms

The flutter mechanisms in the regions above and below Mach 1 are quite different. Here we present an investigation of the mechanisms for a subsonic ($M_\infty = 0.499$, $q_{dyn} = 5900$) and transonic ($M_\infty = 1.0$, $q_{dyn} = 4300$) flutter.

Since the calculations are based on inviscid Euler flow, it is possible to display the local surface Mach number. Figure 5.1 shows the surface geometry and local Mach number distribution for the subsonic and transonic case. The top two images show the Mach number distribution for the steady-state solutions. The middle and bottom four images respectively show the instantaneous surface shape and local Mach number for an equivalent single cycle of flutter. For both the subsonic and transonic single flutter cycles, the top left and bottom right images respectively show the states for maximum and minimum deflection at the wing-tip trailing edge. The other two images show the mean positions with maximum vertical up and down velocities.

For the subsonic, rigid solution, the surface Mach number is roughly constant over the whole upper surface, and is close to the subsonic free stream Mach number. This indicates that there is no shock or expansion wave. For the transonic case, however, there is a soft lambda shock on the upper surface, tracing from the wing-tip leading edge to the wing root trailing edge.

For the cycle of subsonic flutter, the local surface Mach number for each image is in the subsonic region. In the cycle of transonic flutter, at the extreme down position, $t = 0.438$ s, there is near the outer leading edge a region of highly increased local Mach number, indicating an expansion wave. This high Mach number region is broken by a strong shock near the outer half-span of the leading edge. In the same image, a weaker shock propagates in the middle of the surface. At the mean positions, $t = 0.452$ s and $t = 0.482$ s, the instantaneous local Mach distributions are similar to the steady-state, rigid solutions, with the appearance of a soft lambda shock. At the extreme up position, $t = 0.468$ s, there is a sharp local shock wave near the wing-tip leading edge. In reality, adverse pressure gradients caused by these shock or expansion waves, could lead to boundary layer separation. However, these phenomena can not be modeled using inviscid Euler flow.

The strong difference in surface flows between the subsonic and transonic case is reflected in the surface motion and structural dynamics. To characterize the flutter, we look at the timeseries of the total structural energy, $E(t)$. Figure 5.2 shows the modal energy response for the same two, subsonic and transonic flutter cases. For the subsonic case, the modal energy response is entirely in the first and second mode. This behaviour is consistent with that of a typical classical flutter, with a bending-torsion coupling. For the transonic case, however, the motion is dominated by the first structural mode. This produces a drop in flutter frequency, moving closer to the frequency of the first bending mode.

Another feature which distinguishes the transonic and subsonic instabilities is the transition to flutter. The behaviour of the transition is quite different at low speeds compared with transitions near the transonic dip. The slope of

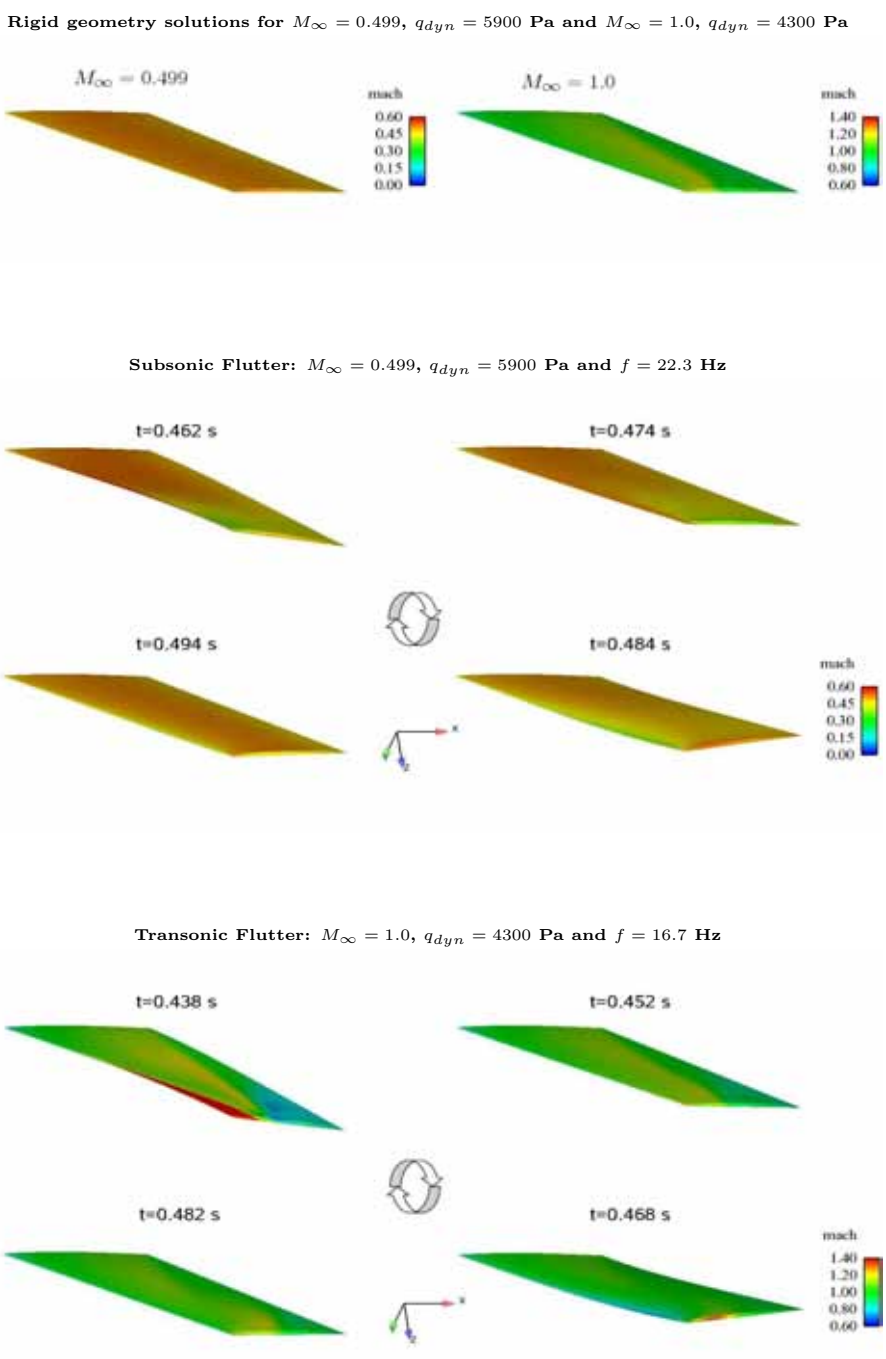

Figure 5.1: Steady-state, surface local Mach number for a subsonic ($M_\infty = 0.499$ and $q_{dyn} = 5900$ Pa) and transonic case ($M_\infty = 1.0$ and $q_{dyn} = 4300$ Pa), together with their corresponding instantaneous surface shape and local Mach number for a single cycle of flutter.

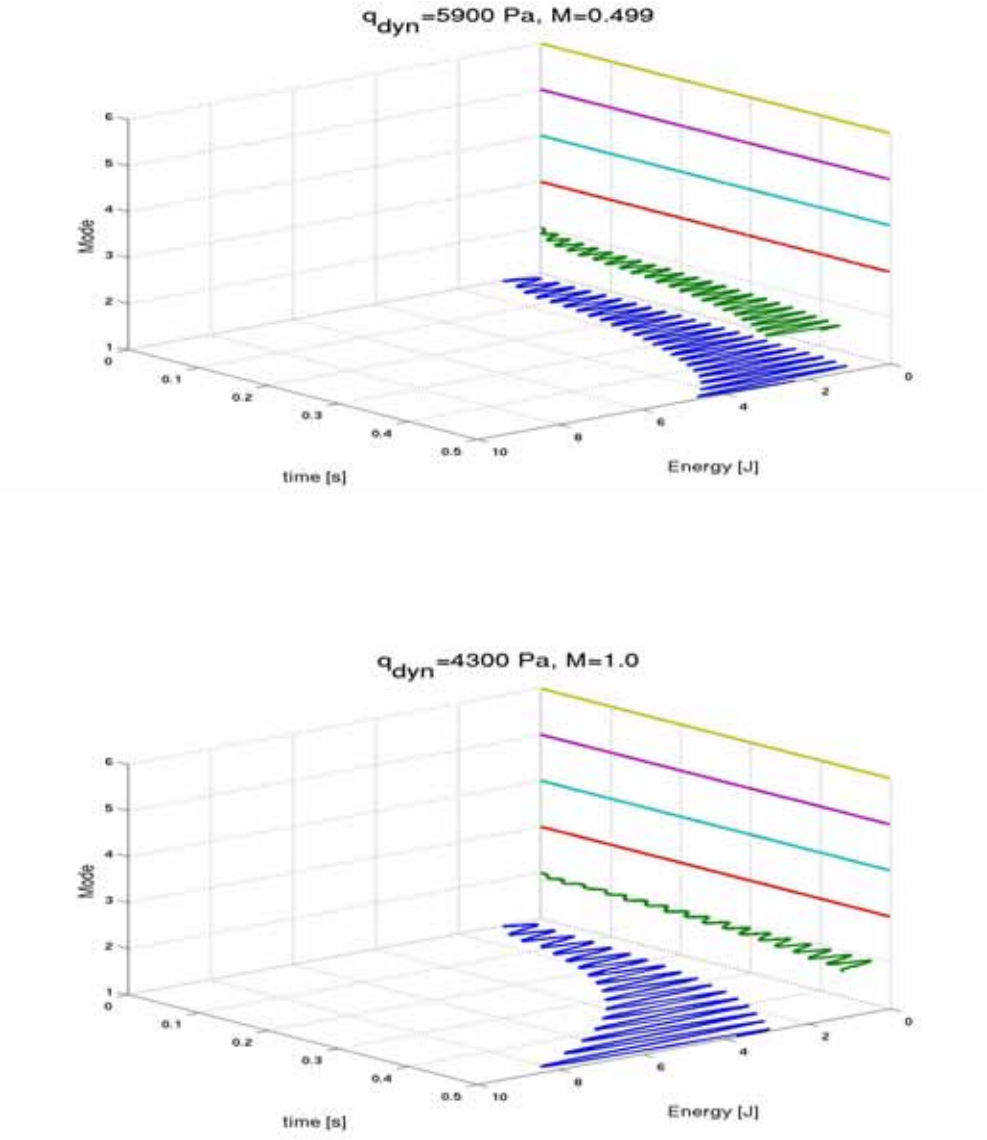

Figure 5.2: Modal flutter energy response for an unstable subsonic ($M_\infty = 0.499$, $q_{dyn} = 5900$) and transonic case ($M_\infty = 1.0$, $q_{dyn} = 4300$ Pa).

the aerodynamic damping versus dynamic pressure curve, (Figure 4.6) as it passes through the flutter dynamic pressure is a qualitative measure of how rapidly the flutter would develop during accelerated flight. Figure 5.3 shows the damping slope at the neutral point, $(\frac{d\zeta_e}{dq})_{\zeta_e=0}$, as a function of the Mach number. From this figure one can see that the absolute value of the slope decreases with a increase in Mach number. Hence, the onset of the transonic flutter is much softer than that of the subsonic "classical" flutter.

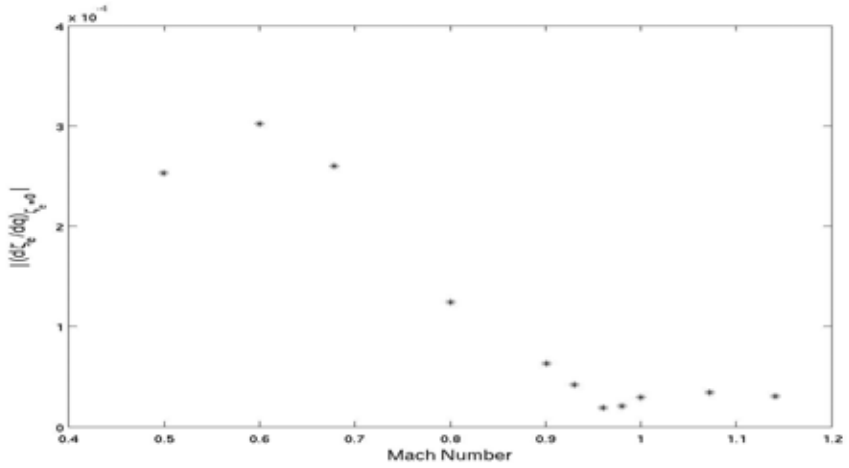

Figure 5.3: Damping slopes at $\zeta_e = 0$.

6 Conclusions and Recommendations

6.1 Conclusions

A comprehensive set of modal coupled aeroelastic simulations has been performed with Edge for a published experimental case: the AGARD 445.6 aeroelastic wind-tunnel model. This work provides additional validation of the aeroelastic implementation as recommended in the previous work of Smith [9].

The computed flutter boundary is generally in good agreement with the experimental data and other similar aeroelastic simulations. The success in modeling the transonic dip in both flutter dynamic pressure and frequency show strong evidence of the flow-solver's ability to model nonlinear fluid-structure interaction.

The flutter characteristics in both subsonic and transonic regimes have been investigated with different analysis methods. These analysis have shown that the dynamic instability in the subsonic regime is characterized as a sharp transition to a classical flutter, with bending-torsion coupling. Increasing the Mach number, there is a smooth transition to a different flutter mechanism, characterized by shock-movement locking in to the first structural bending mode.

The results from Edge for the AGARD 445.6 wing show no evidence of limit cycle oscillations. The absence of these phenomena is consistent with observations in the wind-tunnel experiments and similar aeroelastic simulations. Furthermore, since limit cycle oscillations have been detected with Edge for other models, such as the MDO-wing, we conclude that their absence here is not due to any shortfall in the code or methods used.

The study of the AGARD 445.6 model is the first validation of the modal coupled aeroelastic implementation in Edge with wind-tunnel experiments. The quality of the Edge flutter results for this wing is an adequate validation of the code's aeroelastic functionality.

6.2 Recommendations

Considering the relatively coarse mesh used, the Edge results are strikingly accurate, however, improvements might still be achieved with calculations on a finer grid. In particular, this is indicated by the stagnation zone upstream of the leading edge. From basic aerodynamics we know that the pressure coefficient at a stagnation point is 1. However, in the Edge flow simulation, in the stagnation zone along the leading edge, there are significant deviations from this ideal value, with largest differences above Mach 1. Such behaviour is known to be caused by poor grid resolution. Grid refinement is therefore especially necessary for the leading edge.

A further step could be to include viscosity effects, by using a RANS[1] flow model. RANS calculations would require a prismatic grid and grid size $\sim$ 1 million cells, with computational costs about 50 times of those in the

[1] Reynolds Average Navier Stokes

Euler simulations. However, since the AGARD wing is quite thin, the viscosity effects are small, therefore RANS calculations would probably not result in large improvements in accuracy.

Another element in the computations that could be improved, is the damping estimator. The damping estimation is based on an algorithm that samples the extrema in the impulse response and calculates the damping, assuming an exponential, single-degree of freedom system. This is a good approximation for the AGARD 445.6 wing. It can be argued that there is a need for more sophisticated System Identification models which exploit all the response data. These models would probably not improve the flutter results for the AGARD 445.6 model. They are, however, necessary for more complicated systems, e.g. wing-pylon-nacelle and wings with external stores.

Finding the flutter boundary with Edge required a large set of time-marching calculations with large computational cost. It is therefore desirable to find an alternative to this brute force approach, reducing the computational time whilst maintaining at least the same accuracy. Recently, numerical test procedures based on reduced-order models (ROMs) have been constructed for CFD codes to faster locate the flutter boundary [2]. These models work by capturing the dominant dynamic behaviour of the full set of CFD equations at lower cost, reducing the number of CFD calculations required. These methods are recommended for the future development of Edge.

Aeroelastic wind-tunnel experiments are of prohibitively expensive, therefore nowadays aeroelasticians put more effort in developing codes that could deliver adequate results, thus reducing the need of wind-tunnel experiments. However, validation against wind-tunnel experiments is a necessary step in the development process of any aeroelastic code. Unfortunately, few aeroelastic wind-tunnel experiments are available in the public domain. To further develop the CFD-based, aeroelastic codes, there is a need for more validation studies against different aeroelastic wind-tunnel experiments, especially in the transonic region.

Bibliography

[1] J. Cai, F. Liu, H. M. Tsai, A. S. F. Wong, Y. Zhu, *Calculation of Wing Flutter by a Coupled Fluid-Structure Method*, Journal of Aircraft, Vol. 38, NO. 2, March-April 2001.

[2] L. Cavagna, G Quaranta, P. Mantegazza, *Application of Navier-Stokes simulations for aeroelastic stability assessment in transonic regime*, article in press, computer and Structures (2007), doi:10.1016/j.compstruc.2007.01.005.

[3] Germaine Stanislasse Laure Goura, *Time Marching Analysis of Flutter Using Computational Fluid Dynamics*, Ph.D Thesis, September 2001.

[4] W. Haase, V. Selmin, and B. Winzel (eds.), *Progress in computational Flow-Structure Interaction results of the project UNSI, supported by the European Union 1998-2000*, Notes on Numerical Fluid Mechanics and Multidisciplinary Design (NNFM), vol. 81, Springer-Verlag, 2003, ISBN 3-540-43902-1.

[5] Jones, George W., Jr., and DuBose, Hugh C., *Investigation of Wing Flutter at Transonic Speeds for Six Systematically Varied Wing Plan Form*, NACA RM L53G10a, 1953.

[6] Lee-Raush EM, Batina JT, *Wing Flutter boundary prediction using unsteady Euler aerodynamic method*, NASA Technical Memorandum 107732, March 1993.

[7] Nuno M. M. Maia, Julio M. M. Silva, *Theoretical and Experimental Modal Analysis*, England, 1997.

[8] P. Pahlavanloo, *Dynamic Aeroelastic Simulation of the AGARD 445.6 Wing using Structure-Coupled CFD*, M.Sc. Thesis, KTH, April 2007.

[9] Smith, J., *Aeroelastic Functionality in Edge, Initial implementation and Validation*, Tech. Rep. FOI-R1485-SE, FOI, December 2005.

[10] E. Carson Yates, Jr, *AGARD Dynamic Aeroelastic Configurations for Dynamic Response I-Wing 445.6*, July 1988, ISBN 92-835-0463-1.

[11] W. D. Whetstone, *EISI-EAL Engineering Analysis Language Reference Manual*, Engineering Information Systems, Inc., San Jose, CA, July 1983.

[12] Edge Theoretical Formulation, www.edge.foi.se

FOI is an assignment-based authority under the Ministry of Defence. The core activities are research, method and technology development, as well as studies for the use of defence and security. The organization employs around 1350 people of whom around 950 are researchers. This makes FOI the largest research institute in Sweden. FOI provides its customers with leading expertise in a large number of fields such as security-policy studies and analyses in defence and security, assessment of different types of threats, systems for control and management of crises, protection against and management of hazardous substances, IT-security an the potential of new sensors.

FOI
Swedish Defence Research Agency
SE-164 90 STOCKHOLM

Tel: +46 8 5550 3000
Fax: +46 8 5550 3100

www.foi.se